small method
www.small-methods.com

Emergence of Ferroelectricity in Halide Perovskites

Shamim Shahrokhi, Wenxiu Gao, Yutao Wang, Pradeep Raja Anandan, Md Zahidur Rahaman, Simrjit Singh, Danyang Wang, Claudio Cazorla, Guoliang Yuan, Jun-Ming Liu, and Tom Wu**

Perovskite oxides such as $PbZr_xTi_{1-x}O_3$ (PZT) and $BaTiO_3$ show excellent dielectric, piezoelectric, pyroelectric, and ferroelectric properties simultaneously and have been widely used in capacitor, sensor, actuator, motor, surface acoustic wave devices, and energy storage applications. Recently, a variety of solution-processed halide perovskite materials have been discovered to exhibit fascinating properties such as high charge mobility, strong light absorption, and even ferroelectricity. In this review, the recent progress on two classes of halide perovskite ferroelectrics is summarized. The first class is organo-lead halide perovskite semiconductor such as $MAPbI_3$ ($MA=CH_3NH_3^+$), which is intensively pursued for solar cell and light emitting diode applications. Dynamic ferroelectric polarization is believed to be one of the essential factors to protect carriers from being scattered by charged defects in these halide perovskites. The second class is normal/multilayered halide perovskite ferroelectrics with large polarization or strong piezoelectricity. The piezoelectric coefficient of these latter perovskites can be as high as ≈1540 pC N^{-1}, comparable to those of PZT-based ferroelectrics. Multiaxial polarizations and morphotropic phase boundaries are also demonstrated in such halide perovskites. Overall, the fast development of halide perovskite ferroelectrics opens a new avenue for not only advancing fundamental materials science but also designing novel electronic and photoelectric devices.

1. Introduction

Discovered in 1921, ferroelectricity was initially called Seignette electricity because Seignette or Rochelle Salt was the first material that was found to exhibit ferroelectric properties.[1] From a crystallographic point of view, ferroelectric materials are characterized by the breaking of inversion symmetry, that is, they are non-centrosymmetric.[2] As a result, each ferroelectric material exhibits a macroscopic polarization that can be switched by an external electric field. Many well-known inorganic ferroelectrics possess perovskite structure and can be described with the general chemical formula of ABO_3, where A and B represent cations of different sizes and B is a transition metal (e.g., $BaTiO_3$ and $PbTiO_3$).[3]

Perovskite oxide ferroelectrics have been extensively used in capacitor, sensor, actuator, memories, energy storage, surface acoustic wave devices, optoelectronics, and microelectromechanical systems applications, which are critical components for modern technologies. For example, $BaTiO_3$ has been widely used in capacitor applications since 1950.[4] Many ferroelectrics also have high dielectric constant, low dielectric loss, and high breakdown electric field, showing high electric energy density and storage efficiency during energy storage as capacitors.[5] $PbZr_xTi_{1-x}O_3$ (PZT) has been incorporated in automobiles as piezoelectric sensors,[6] and it is also used in actuators for the direct conversion of electrical energy to mechanical energy which are especially important for robotics, optical fiber switches and optical displays.[7] Ferroelectric random-access memories (RAMs) are another application of perovskite oxide ferroelectrics such as PZT and doped $Bi_{4-x}A_xTi_3O_{12}$ (A = La, Nd, et al),[8] which have the merits of their high speed, nonvolatility, low power requirements, anti-radiation, physical robustness, and high density. Besides, $LiNbO_3$ and $LiTaO_3$ have been widely used as surface acoustic wave devices, which are the key components of wireless communication devices such as TV and mobile phone. Nevertheless, perovskite oxide ferroelectrics, although have been used in various applications, present some disadvantages. For instance, most of them may contain heavy metals which are not environmentally friendly and are usually processed at high temperatures. In addition, most perovskite oxide ferroelectrics are brittle, hence they cannot be exploited in flexible devices.[9]

S. Shahrokhi, Y. Wang, P. R. Anandan, Md Z. Rahaman, Dr. S. Singh, Dr. D. Wang, Dr. C. Cazorla, Prof. T. Wu
School of Materials Science and Engineering
Faculty of Science
University of New South Wales
Sydney 2052, Australia
E-mail: tom.wu@unsw.edu.au

Dr. W. Gao, Prof. G. Yuan
School of Materials Science and Engineering
Nanjing University of Science and Technology
Nanjing 210094, China
E-mail: yuanguoliang@njust.edu.cn

Prof. J.-M. Liu
Laboratory of Solid State Microstructure and Innovation Center of Advanced Microstructures
Nanjing University
Nanjing 210093, China

The ORCID identification number(s) for the author(s) of this article can be found under https://doi.org/10.1002/smtd.202000149.

DOI: 10.1002/smtd.202000149

Halide perovskites, with general chemical formulas of 3D ABX_3 and layered 2D $A_{n+1}B_nX_{3n+1}$ (X = F, Cl, Br, or I), consist of inorganic BX_6 octahedra, with A, an organic/inorganic cation (e.g., Cs or MA = $CH_3NH_3^+$) and B usually a metal cation with smaller size (e.g., Pb^{2+} or Sn^{2+}).[10] Halide perovskites exhibit many unique properties that cannot be observed in perovskite oxide ferroelectrics, such as structural softness, lightweight, and low synthesis temperatures (**Table 1**).[11] On the other hand, the existence of ferroelectricity in halide perovskites remains controversial and a long-lasting theme of research. For example, whether $CH_3NH_3PbI_3$ ($MAPbI_3$) truly exhibits ferroelectricity or not remains contentious. Piezoelectric force microscopy (PFM) and scanning electron microscopy studies reported polar domains in tetragonal $MAPbI_3$, and a weak ferroelectricity was demonstrated by dielectric and piezoelectric measurements as well as second harmonic generation (SHG).[12] However, most traditional methods which are effective to identify ferroelectric insulators cannot effectively characterize the ferroelectricity of a typical semiconductor like $MAPbI_3$. It is not easy to differentiate ferroelectric domains from ferroelastic domains, and a standard saturated polarization versus electric field (P–E) loops has not been achieved in $MAPbI_3$ until now.[13] It was reported by macroscale polarization and temperature-dependent dielectric measurements that $MAPbI_3$ thin films cannot be ferroelectric under solar cell measurement conditions.[17] Obviously, there is a vast space for researchers to develop new characterization techniques and to prepare reliable ferroelectric semiconductors.

Clarifying the possibility of existence of ferroelectricity in halide perovskites is not just a question of fundamental interest, it may also have important technological consequences. For example, some theoretical works have shown that ferroelectric nanodomains can reduce the recombination of light-excited electron–hole pairs, extend the carrier lifetime and promote the charge separation and collection.[14] This unique merit of $MAPbI_3$ contributes to its promising optoelectronic properties such as high carrier mobility, tunable light absorption, long charge diffusion lengths, and high power conversion efficiency (PCE) of >20% in the corresponding solar cells.[3]

On the other hand, a series of halide perovskite ferroelectrics with Curie temperature above 373 K have been discovered recently, and some of them show excellent ferroelectric and piezoelectric properties (Table 1). For example, Liao et al. synthesized the molecular perovskite $(TF)_{0.26}(TC)_{0.74}CdCl_3$ with morphotropic phase boundaries (MPB) of monoclinic and hexagonal phases.[15] It shows the maximum piezoelectric coefficient d_{33} of ≈1540 pC N^{-1} at room temperature, which is even higher than most conventional ferroelectrics, thus possessing the potential to be used in flexible piezoelectric applications.

In this progress report, we will first discuss briefly the fundamentals of ferroelectric materials, and then we introduce several organo-lead halide perovskite semiconductors with a focus on the elusive ferroelectricity and the impact of such a ferroelectric-like property on the photovoltaic applications, particularly solar cells. Moreover, a series of halide perovskite ferroelectrics with strong piezoelectricity and poor semiconducting properties are reviewed and compared to the organo-lead halide perovskites. Finally, we present perspectives on future research directions to advance halide perovskite ferroelectrics.

Shamim Shahrokhi is currently a Ph.D. student in the Department of Materials Science and Engineering, University of New South Wales (UNSW), Sydney, Australia. She received her bachelor and master degrees in metallurgy and materials engineering from University of Tehran, Iran in 2015 and 2017, respectively. Her research is focused on the dielectric, optoelectronic, and photoelectrochemical properties of hybrid halide perovskite materials.

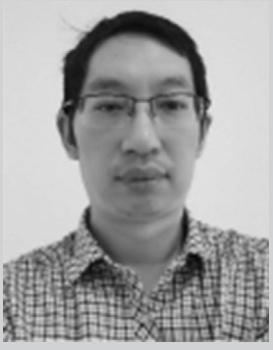

Guoliang Yuan is currently a professor in the School of Materials Science and Engineering, Nanjing University of Science and Technology, China. He received his Ph.D. degree from Nanjing University in 2004. Then, he joined the Department of Applied Physics, The Hong Kong Polytechnic University and worked as an Alexander von Homboldt research fellow in Bonn University from 2006 to 2007 and JSPS research fellow in Tsukuba University from 2008 to 2009. He joined Nanjing University of Science and Technology in 2009. His research focuses on ferroelectric, piezoelectric, and multiferroic thin films and devices.

Tom Wu received his B.S. degree from Zhejiang University in 1995 and Ph.D. degree from the University of Maryland, College Park in 2002. Before joining University of New South Wales (UNSW) in Sydney as a full professor, he worked as a postdoc in Argonne National Laboratory in Chicago, assistant professor in Nanyang Technological University (NTU) Singapore, and associate professor in King Abdullah University of Science and Technology (KAUST). Dr. Wu works in the areas of oxide thin films, nanomaterials, and hybrid perovskites, with a focus on their electronic, magnetic, and optical functionalities.

Table 1. Basic physical properties of halide perovskite materials, and some representative ferroelectric oxides are also shown for comparison. Here, MD is *N*-methyl-*N*′-diazabicyclo[2.2.2]octonium, TF is trimethylfluoromethyl ammonium, TC is trimethylchloromethyl ammonium, PEA is 2-phenylethylammonium, EA is ethylammonium, R_2PbI_4 is [-(4-chlorophenyl)ethylammonium]$_2PbI_4$, S_2PbI_4 is [-1-(4-chlorophenyl) ethylammonium]$_2PbI_4$, D_2PbI_4 is (4,4-difluorocyclohexylammonium)$_2$ PbI_4, T_C is ferroelectric Curie temperature, P_s is spontaneous polarization, d_{33} is piezoelectric coefficient, E_g is the bandgap of a semiconductor, L_D is minority carrier diffusion length, J_{SC} is the short-circuit current density of a solar cell, MA is Methylammonium, and FA is Formamidinium.

Material	Crystal structure	T_C [K]	P_s [μC cm^{-2}]	d_{33} [pC N^{-1}]	E_g [eV]	L_D [μm]	PCE or J_{SC}	Ref.
$MAPbI_3$ film	tetragonal I4*cm*	327	–	–	1.55	>100	PCE ≈ 20%	[12]
$MAPbI_{3-x}Br_x$ (x = 0–1.5)	tetragonal I4*cm*	–	–	–	1.55–1.83		PCE ≈ 14%	[16]
$MAPbI_{3-x}Cl_x$ film	tetragonal I4*cm*	–	–	–	1.55–1.6	>1	PCE ≈ 19%	[17]
$MAPb_{1-x}Fe_xI_3$ (x = 0–0.07)	tetragonal I4*cm*	–	≈2	–	–	–	–	[18]
$FAPbBr_3$	close to cubic P*m*–3*m*	–	–	25 pm V^{-1}	2.27	107	PCE ≈ 6.1%	[19]
$FASnI_3$	orthorhombic *Amm2*	–	–	–	1.37	–	PCE ≈ 8.9%	[20]
$CsPbBr_3$ (under 15 GPa)	tetragonal P4*mm*	–	23	–	≈2.1	>9.2	PCE ≈ 7.78%	[21]
$CsPbF_3$	rhombohedral *R3c* (theory)	–	–	–	–	–	–	[22]
$(PEA)_2(MA)_4$ Pb_5I_{16}	-	444	≈0.25	–	–	–	–	[23]
$(EA)_4Pb_3Br_{10}$ crystal	orthorhombic P2*cb*	374	3	–	2.7	–	I_{SC} ≈ 15 nA	[24]
$(EA)_2(MA)_2Pb_3Br_{10}$ crystal	orthorhombic $Cmc2_1$	375	3.7	–	2.7	–	J_{SC} ≈ 4.1 μA cm^{-2}	[25]
MD-NH_4I_3 crystal	rhombohedral R_3	448	19	14	–	–	–	[26]
TC-$MnCl_3$ crystal	triclinic *Cc*	406	4	185	–	–	–	[27]
$(TF)_{0.26}(TC)_{0.74}CdCl_3$ crystal	triclinic *Cc*, hexagonal $P6_3/m$	≈370	≈8	1540	–	–	–	[15]
R_2PbI_4 crystal	triclinic P_1	383	13.96	3	2.34	–	–	[28]
S_2PbI_4 crystal	triclinic P_1	373.2	13.96	3	2.34	–	–	[28]
D_2PbI_4 crystal	orthorhombic $Cmc2_1$	377	–	–	2.38	–	I_{SC} ≈ 1.4 pA	[29]
$PbZr_{0.52}Ti_{0.48}O_3$ film	rhombohedral *R3c*, tetragonal P4*mm*	≈623	≈60	≈300	≈3.5	–	J_{SC} ≈ 0.008 μA cm^{-2}	[30]
$BaTiO_3$ film	tetragonal P4*mm*	390	24	190	3.2	–	J_{SC} ≈ 5 μA cm^{-2}	[31]
$BiFeO_3$ film	rhombohedral *R3c*	1086	≈110	≈90 pm V^{-1}	≈2.8	–	J_{SC} ≈ 0.3 μA cm^{-2}	[32]
Bi_2FeCrO_6 film	rhombohedral *R3*	–	>20	–	1.39–2.6	–	PCE ≈ 4%	[33]

2. Brief Introduction of Ferroelectric Materials

2.1. Basic Physics of Ferroelectricity

Ferroelectric materials are a subclass of pyroelectrics, which are a subclass of piezoelectrics and they are all a group of dielectric materials (**Figure 1**a).[34] Therefore, ferroelectrics possess both the pyroelectric and piezoelectric properties and are known as wide-bandgap polarizable semiconductors.[35] According to the definition, ferroelectric compounds must adopt symmetry-breaking space groups belonging to the 10 polar point groups, that is, triclinic 1 (C_1), monoclinic *m* (C_s), 2 (C_2), orthorhombic *mm*2 (C_{2v}), trigonal 3 (C_3), 3*m* (C_{3v}), tetragonal 4 (C_4), 4*mm* (C_{4v}), hexagonal 6 (C_6), and 6*mm* (C_{6v}) (Table 1 and Figure 1b). Although ferroelectricity is believed to be a property of crystalline solid compounds according to the conventional wisdom, it was also discovered in liquid crystals. For example, it was shown that C and H liquid crystals with monoclinic symmetry consisting of chiral molecules can possess spontaneous polarization.[36]

Ferroelectricity is the ability of a material to have a spontaneous polarization (P) which can be switched to different orientations under an external electric field (E) (**Figure 2**a). P is dependent not only on E but also on its history, yielding a P–E hysteresis loop which resembles to the M–H hysteresis loops of ferromagnetic materials. Ferroelectric materials typically consist of many small microscopic regions with homogenous polarizations inside each region (i.e., domain), and the macroscopic P is zero when the domains are oriented randomly. The polarizations of these domains tend to orient along E when this is larger than coercive field (E_c) and eventually saturated polarization (P_s) is achieved that does not change under further increase of the electric bias along the OABC curve (Figure 2a).[35a] When the external electric field is decreased, the polarization of some domains decreases along the CD curve (i.e., depolarization), however a remanent polarization (P_r) remains upon full removal of the electric bias due to kinetics arrest of polar domain switching (i.e., certain energy barriers need to be overcome) (Figure 2a).[37]

In the absence of external electric fields, ferroelectric materials undergo a transition from a ferroelectric phase to a paraelectric phase at the Curie temperature (T_c). The classification of the ferroelectric–paraelectric phase transitions is based on the nature of phase change occurring at T_c, including displacive type and order-disorder type (Figure 2b). Many inorganic oxides such as $BaTiO_3$ belong to the displacive type, in which relative displacement of the ions creates a spontaneous polarization. On the other hand, $NaNO_2$ is a typical ferroelectric of order-disorder type, in which reorientation of the dipolar NO_2 ions generates ferroelectricity. In fact, the two types are not mutually

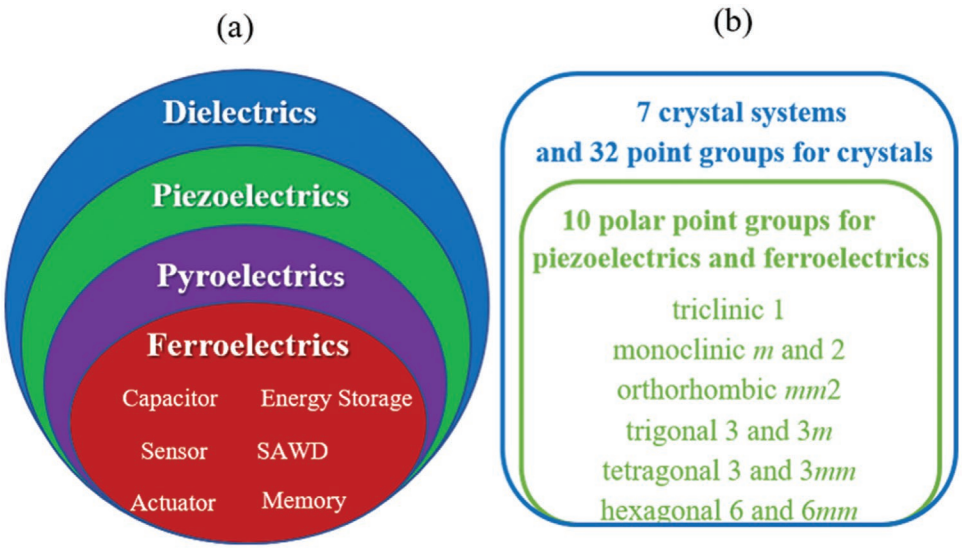

Figure 1. a) Relationship of dielectric, piezoelectric, pyroelectric, and ferroelectric materials. b) Crystal systems and point groups of ferroelectrics.

exclusive and some ferroelectric crystals show both displacive and order-disorder characteristics.[34c]

2.2. Techniques of Measuring Ferroelectric Materials

In the past decades, ferroelectric insulators have been studied extensively and several effective methods were developed to identify whether a new material shows ferroelectricity or not. In addition to an asymmetrical crystal structure, a ferroelectric material shows ferroelectricity, piezoelectricity, and pyroelectricity simultaneously. Thus, these four properties can be characterized to identify ferroelectricity of a new material. First, all ferroelectrics have the asymmetric crystal structures with 10 polar point groups, which can be characterized by techniques such as XRD, SHG, TEM, and other advanced microscopies.[8,34c] These methods are quite effective if the polarization of the specimen is larger than 1 μC cm^{-2}. Second, ferroelectricity is commonly characterized by *P*–*E* hysteresis loop. When an *E* over E_C is applied on an insulating ferroelectric material, polarization can switch its orientation, which introduces the change of positive and negative bound charges at two opposite surfaces. As a result, there are free charges to neutralize the new bound charges. For a ferroelectric insulator, nearly all free charges go through an external circuit and thus a commercial ferroelectric tester can integrate the external current and time to calculate the bound charges and the corresponding polarization. Third, a d_{33} meter is commonly applied to characterize the piezoelectric effect with a unit of pC N^{-1}. The mechanical force can introduce a change in the surface-bound charges of two opposite surfaces as well as the corresponding external current. Furthermore, a strain meter is commonly used to characterize the inverse piezoelectric effect with a unit of pm V^{-1} when an external *E* induces the nonlinear strain of a material. Both Doppler instrument and PFM as strain meters are widely applied to identify strain with an accuracy of pm or better,[9,38] and different kinds of domains have recently been discovered by PFM.[12,15,23–33] Finally, the bound

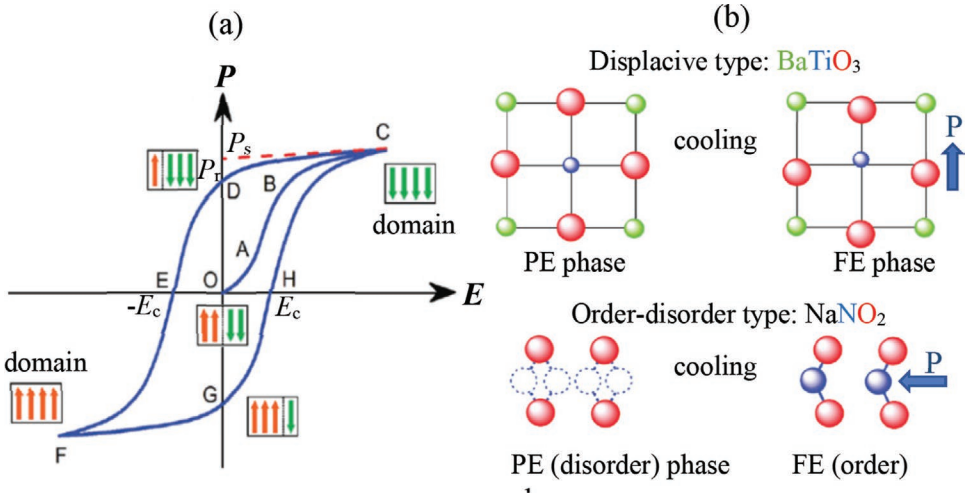

Figure 2. a) *P*–*E* hysteresis loops and the domain evolution during polarization switching. b) Schematic illustrations for the displacive-type and order-disorder-type ferroelectric–paraelectric phase transition.

charges of two opposite surfaces will vary with the temperature changing in a pyroelectric material, and thus there are free charges to neutralize these new bound charges. Through integrating the pyroelectric current and time, the total free charges and the corresponding polarization can be calculated. In fact, this method has successfully discovered many new multiferroic materials with narrow bandgaps and polarizations as small as $\approx 10^{-5}$ μC cm^{-2}.[39]

Although these traditional characteristic methods are effective for ferroelectric insulators, it is still a big challenge to exactly identify some ferroelectric semiconductors with halide perovskite structure such as $MAPbI_3$. Indeed, $MAPbI_3$ and many halide perovskites do not show large polarization. Besides, there is just slight difference between their asymmetric and symmetric crystal structures which makes it difficult to identify this difference by normal XRD, TEM, SHG, and so on. Moreover, many halide perovskite materials are not stable enough during TEM measurements.[8,34c] Most importantly, when there is a change in polarization and the corresponding surface bound charges induced by the varying *E*, strain, and/or temperature, the free charges inside semiconductor can replace the free charges in external circuit to neutralize the new bound charges. As a result, polarization cannot be exactly calculated through integrating external current and time. Besides, the inner current inside semiconductor may produce heat which is large enough to break the semiconductor itself. Recently, the domains of halide perovskites such as $MAPbI_3$ have clearly been observed by PFM,[12,16,18–21,38] however it is not easy to switch their polarization by an external *E*. In fact, an *E* may induce a large current to break semiconductor before reaching above E_C to switch the polarization. In this case, it is not easy to differentiate ferroelectric domains from ferroelastic domains due to inhomogeneous strain. Although there are many obstacles, a great deal of work has already been performed and it is possible to clearly switch and manipulate polarization in most of the ferroelectric semiconductors.

3. Lead-Halide Perovskite Semiconductors with Weak Ferroelectricity

3.1. Ferroelectric Large Polaron

Lead-halide perovskite materials can be prepared with the aqueous solution method at room temperature, and some of them have been extensively applied in solar cells and light emitted diodes (LED).[40] The crystal structure of halide perovskites is presented in **Figure 3**a. Recently, extensive efforts have been devoted to improving the efficiency of perovskite solar cells, especially by composition engineering and optimizing the material processing (Figure 3b). Despite of having high defect densities, prototype halide perovskites such as $MAPbI_3$, $CH(NH_2)_2PbI_3$ (i.e., $FAPbI_3$), and $CsPbBr_3$, exhibit excellent charge transport properties like conventional semiconductors with 7N or higher purity (e.g., Si and GaAs).[41] First, the temperature (*T*) dependence of charge carrier mobility (μ) follows a simple power law ($\mu \propto T^{-3/2}$), thus indicating the hindrance of coherent transport by acoustic phonon scattering in the halide perovskites.[40] Second, halide perovskites possess a modest charge carrier mobility ($\mu \approx$ 1–100 cm^2 V^{-1} · s^{-1}), a high carrier diffusion length (up to 10^2 μm), and a long carrier lifetime (≥1 ms) simultaneously.[42] Third, the electron–hole recombination rate constant (10^{-10} cm^3 s^{-1}) is as low as those of the purest crystalline semiconductors such as GaAs.[43] These properties of hybrid organic–inorganic lead halide perovskites indicate that there are few scatterings of charge carriers by charged defects, optical phonons, or other interferences.

Recently, Zhu and Podzorov et al. proposed that the screened Coulomb potential created in the crystal by large polarons can reduce the carrier scattering by charged defects, other charge carriers, and phonons.[41b,c] There are two kinds of large polaron that can protect charge carriers from scattering, that is, Fröhlich large polaron and ferroelectric large polaron. For the Fröhlich large polaron, the polarization of the ionic lattice (i.e., the dipole moment due to atomic displacement from their equilibrium position) shows a linear response to the applied electric field or generated by charged defects. As a result, the dipole moment in a unit cell decreases with increasing the distance from the injected charge (Figure 3c). For the ferroelectric large polaron model (Figure 3d), there is an enhanced local electric field of 0.1–1 MV cm^{-1} in the proximity of a charge, which can induce collective polarization and polar nanodomains (PND) in the ferroelectric-like materials. These nanodomains may be dynamic and transient and vanish when the charge is removed and there is just a local microscopic ordering with radial symmetry centered on the charge, which is different from the conventional ferroelectric phenomenon.[41c] Compared with a conventional Fröhlich large polaron, much larger Coulomb potential screening is caused by the ferroelectric large polaron. Furthermore, there is a chance for inducing a potential barrier against charge recombination due to the collective polarization of nanodomains. Ferroelectric large polaron model provides a new platform for hybrid perovskite-based defect-tolerant semiconductor devices.

3.2. Impact of Ferroelectricity on Optoelectronic Performance

Ferroelectric properties of halide perovskites can lead to advantageous applications in optoelectronic devices. The impact of ferroelectricity on the performance of energy-conversion devices such as high-performance ferroelectric solar cells has been intensively investigated.[45] In addition, by utilizing ferroelectric semiconductors, photocatalytic activities can be improved with a permanent internal polarization to effectively separate photoexcited carriers.[46] Recently, Singh et al. reported improved photoelectrochemical properties by growing Ag, Nb-codoped $SrTiO_3$ (Ag/Nb:STO) with ferroelectric nanoporous/nanocolumnar structure.[47] By applying external electrical bias, the photocurrent was increased from 40 to 130 μA · cm^{-2} followed by a decrease in flat-band potential from −0.55 to −1.13 V, resulting in an enhanced charge transfer. In addition, Wang et al. reported $EA_4Pb_3Cl_{10}$ (EA = ethylammonium) as a 2D trilayered hybrid perovskite ferroelectric, presenting a high Curie temperature of 415 K and P_s of ≈4.5 μC · cm^{-2} as well as a wide bandgap of 3.39 eV, suitable for applications such as self-powered photodetection.[48] In another work, $(EA)_2(MA)_2Pb_3Br_{10}$ was shown to have ferroelectric behavior with a high Curie

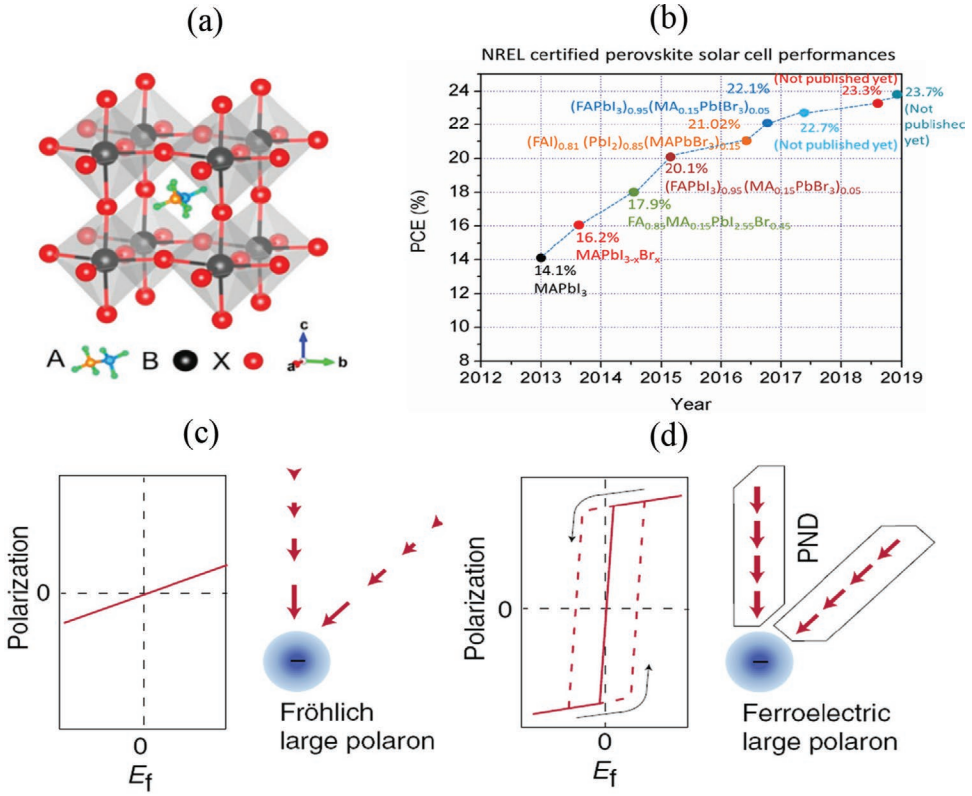

Figure 3. a) Crystal structure of halide perovskite. b) Power conversion efficiency (PCE) of halide perovskite solar cells certified by the U.S. National Renewable Energy Laboratory. Reproduced with permission.[44] Copyright 2019, American Chemical Society. c) Left: *P–E* loops in a conventional crystal. Right: A Fröhlich large polaron where the dipole moment (red arrows) in a unit cell decreases with the distance from the extra charge (blue sphere). d) Left: *P–E* loop in a ferroelectric-like material. Right: a ferroelectric large polaron where dipole moments inside a polar nanodomain (PND) are evenly affected by the extra charge. Reproduced with permission.[41c] Copyright 2018, Macmillan Publishers Limited, part of Springer Nature.

temperature of 375 K, P_s of 3.7 μC · cm^{-2}, and a high photocurrent density of 4.1 μA · cm^{-2},[25] superior to some ferroelectric oxides such as $BiFeO_3$.[49]

In general, hybrid organic–inorganic perovskites with ferroelectric or ferroelectric-like properties have been widely pursued in many applications. Because of their unique low temperature process ability and low manufacture cost, these halide perovskites could be good candidates for future applications, such as flexible and wearable devices.

Among different organic–inorganic perovskites, $MAPbI_3$ and its compositional variants have been widely investigated in photovoltaic (PV) applications due to its promising optical and electronic properties, such as high carrier mobility, strong light absorption, reduced charge recombination, and optimized charge diffusion length. $MAPbI_3$ undergoes two phase transitions, that is, from orthorhombic (space group *Pna2*) to tetragonal (β structure, space group I4/*mcm*) at 162 K and from tetragonal to cubic (α structure, space group *Pm3m*) at 327 K.[50] **Figure 4**a shows the phase transitions of $MAPbI_3$ in comparison to $MAPbBr_3$ and $MAPbCl_3$, depicted from anomalous changes in temperature-dependent dielectric permittivity. Strong evidences of ferroelectricity have been shown for $MAPbI_3$. First, Monte Carlo model simulations suggest the existence of ferroelectricity due to the orientation of the molecular cations following ferreoelectric domains.[51] Second, noncentrosymmetry and pyroelectricity of the tetragonal $MAPbI_3$ film were confirmed by SHG and the abnormal pyroelectric current, respectively. Third, dependence of real (ε') and the imaginary (ε_{im}) relative permittivity as a function of temperature shows a dielectric anomaly around $T_c \approx 327$ K for polycrystalline $MAPbI_3$ films, which suggests the tetragonal $MAPbI_3$ film is ferroelectric. Fourth, exotic dielectric properties are derived in this material due to the presence of MA^+ cations with a large dielectric constant on the order of 10^1–10^3 in the frequency range of 10^{-1}–10^3 Hz.[52] It is believed that MA^+ ions undergo order-disorder phase transition at T_c and mainly introduce the weak ferroelectric polarization along [001] orientation in the tetragonal $MAPbI_3$. At last, the dielectric response is dominated by ε_{im} in this ferroelectric semiconductor. Rakita et al. obtained a *P–E* hysteresis loop from integration of ε_{im} over the bias electric field (E_{DC}) at 204 K (Figure 4b).[4,12,53] Even so, reliable remnant polarization has not yet been experimentally observed in $MAPbI_3$ semiconductor at room temperature until now due to the relatively high electrical conductance and low stability under high applied bias voltage.[54]

Ferroelectric domains were observed in the tetragonal $MAPbI_3$ films with different methods. By chemical etching of the crystal with acetone, Rakita et al. observed polar domains periodically stacked along the polar axis of the crystal.[12] Furthermore, Röhm et al. observed ferroelectric domains by PFM.[55] Ferroelectric domains of alternating polarization with a width of 90 nm were identified (Figure 4c). The polarized

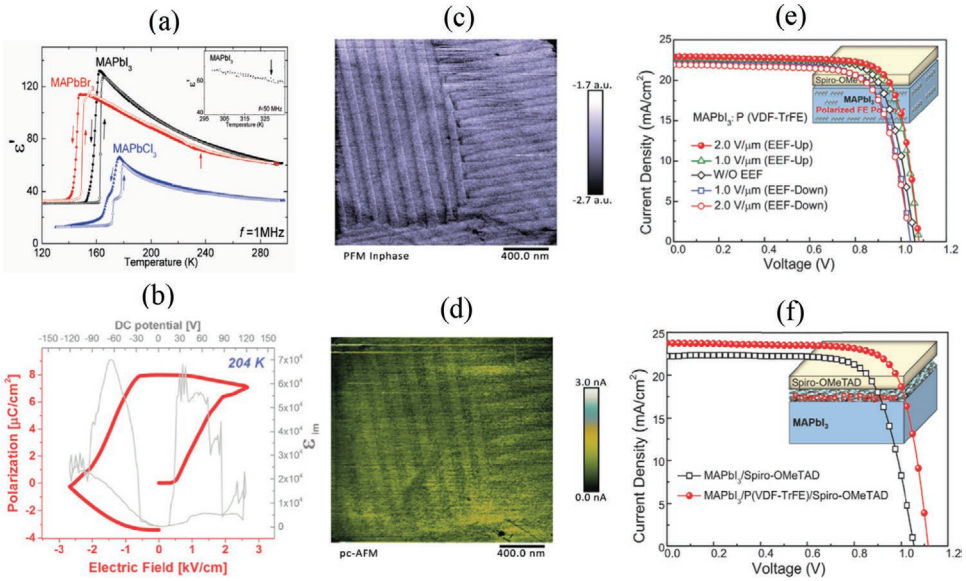

Figure 4. a) The real part ε' of the dielectric permittivity of $MAPbI_3$ and $MAPbBr_3$ single crystals in comparison to $MAPbCl_3$ polycrystal versus temperature at 1 MHz. The inset represents the ε' of $MAPbI_3$ above room temperature at 50 MHz. Reproduced with permission.[50] Copyright 2017, Advanced Energy Materials. b) *P–E* hysteresis loop from integration of ε_{im} over E_{DC}. Reproduced with permission.[12] Copyright 2017, National Academy of Sciences. c) In-plane PFM amplitude image and d) photo-conductive AFM image of a β-$MAPbI_3$ film. Reproduced with permission.[55] Copyright 2017, the Royal Society of Chemistry. e) *J–V* curves in P(VDF-TrFE)-doped $MAPbI_3$ solar cells dependent on varied intensity and direction of external electric field (EEF). f) *J–V* curves in $MAPbI_3$ and $MAPbI_3$/P(VDF-TrFE)-based perovskite solar cells. Reproduced with permission.[60] Copyright 2019, WILEY-VCH Verlag GmbH & Co. KGaA, Weinheim.

domains in one grain with parallel stripes of polarization are able to self-organize to reduce the mechanical strain during cubic to tetragonal or orthorhombic phase transformation.[56] 90° continuation of the polarization pattern within one grain is observed occasionally. The high-resolution photo-conductive atomic force micrographs under illumination also show alternating charge carrier extraction patterns which are due to the local vertical polarization components within the ferroelectric domains (Figure 4d). On the other hand, it was observed that the ferroic domains in $MAPbI_3$ may include alternating polar and nonpolar orders. These domains cannot be switched under an electrical field due to the blockage of polar switchable domains by nonpolar ones.[38] Later, first-principle calculations reveal that ferroelectric domain walls can reduce the bandgaps significantly, as well as promote the charge separation.[23,57] Ferroelectric domain walls improve the conductance of perovskites owing to the reduced bandgap.[58] According to Frost et al., polarized ferroelectric domains in β-$MAPbI_3$ films can act as small internal p-n junctions, which may accelerate the separation of photoexcited electron–hole pairs.[59]

To further improve the cell performance of $MAPbI_3$-based solar cells, Zhang et al. integrated P(VDF-TrFE), a ferroelectric polymer, into the light absorption layer of $MAPbI_3$ and/or between $MAPbI_3$ and the hole-transporting layer of Spiro-OMeTAD.[60] These composite materials effectively improve the crystallization of $MAPbI_3$, enhance the built-in electric field (E_{bi}) and decrease the nonradiative recombination of electron–hole pairs in perovskite solar cells. The P(VDF-TrFE)-doped $MAPbI_3$ shows an orderly arrangement of MA^+ cations, resulting in a preferred growth orientation of polycrystalline perovskite films with reduced trap states. In addition, the depletion region is widened and E_{bi} is enhanced in the device. The photovoltaic performance and polarization of P(VDF-TrFE) was obviously affected by the applied electric field, as shown in Figure 4e. The up-polarization had a positive effect on the cell efficiency, while the down-polarization showed an opposite effect. Most importantly, P(VDF-TrFE) as an interfacial dipole layer plays a critical role in increasing E_{bi}, which enhances the open circuit voltage (V_{OC}) from 1 to 1.14 V due to efficient suppression of nonradiative recombination. Consequently, the resulting perovskite solar cells present a power conversion efficiency of 21.38% (Figure 4f).

3.3. Ferroelectricity of Composition-Tailored Hybrid Perovskite Films

In general, there are several composition-based routes to tuning the ferroelectricity of $MAPbI_3$.[61] By incorporation of Br in $MAPbI_3$, the band gap of iodide-based hybrid perovskites can be adjusted as a result of structural distortion of Pb—I bonds.[62] Furthermore, the improvement of diffusion lengths, carrier lifetimes, and better stability can be achieved by tuning the percentage of $PbBr_2$ in mixed hybrid perovskites.[63]

In a recent work, the ferroelectricity of $MAPbI_{3-x}Br_x$ (x = 0–1.5) was confirmed by PFM.[16] Fully polarization switching was demonstrated by a phase angle difference of 180° in the phase hysteresis loops (**Figure 5**a) and the butterfly-like shape observed in the amplitude loops at the bias-off state. Then the *J–V* characteristics of glass/ITO/PEDOT:PSS/$MAPbI_{1.5}Br_{1.5}$/PCBM solar cells were studied, showing that the polarization switching can change the power conversion efficiencies

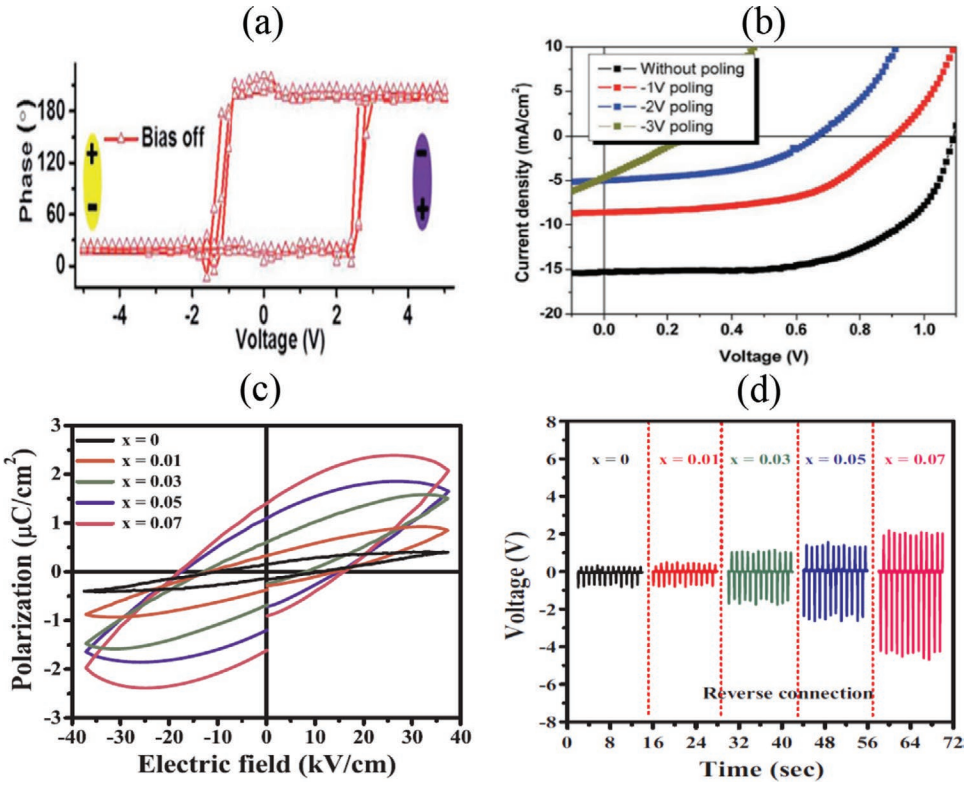

Figure 5. a) PFM Phase versus tip bias of $MAPbI_{1.5}Br_{1.5}$ film, b) *J–V* characteristics of glass/ITO/PEDOT:PSS/$MAPbI_{1.5}Br_{1.5}$/PCBM solar cells under AM1.5 illumination when $MAPbI_{1.5}Br_{1.5}$ film was polarized by negative biases. Reproduced with permission.[16] Copyright 2018, the Royal Society of Chemistry. c) *P–E* loop of $MAPb_{1-x}Fe_xI_3$ ($0 \le x \le 0.07$), and d) output voltage of the flexible PET/ITO/$MAPb_{1-x}Fe_xI_3$/PDMS/Au/PI piezoelectric generators. Reproduced with permission.[18] Copyright 2018, Elsevier Ltd.

(Figure 5b). Besides, Chen et al. investigated a ferroelectric $TiO_2/MAPbI_{3-x}Cl_x$/Au solar cell and observed a high PCE of 19%.[64] Furthermore, the partial replacement of Pb^{2+} with Fe^{2+} improved both the morphology and crystallinity of $MAPb_{1-x}Fe_xI_3$ ($0.01 \le x \le 0.50$) films that undergo a tetragonal-cubic phase transition with a specific Fe^{2+} concentration of $x > 0.07$.[18] The $MAPb_{1-x}Fe_xI_3$ ($x = 0.07$) films exhibited the saturated ferroelectric *P–E* hysteresis loops and a remnant polarization of ≈1.6 μC cm^{-2} (Figure 5c). The flexible PET/ITO/$MAPb_{0.93}Fe_{0.07}I_3$/PDMS/Au/PI generators have an output voltage of ≈7.29 V and a current density of ≈0.88 μA cm^{-2} through the piezoelectric effect of $MAPb_{0.93}Fe_{0.07}I_3$ during its repetitive stretching and bending (Figure 5d).

3.4. Ferroelectricity of $FAPbBr_3$ and Its Derivatives

$FAPbBr_3$ perovskite could be a promising ferroelectric material in high performance energy harvesting applications.[65] PFM measurements revealed that $FAPbBr_3$ nanoparticles contain well-developed ferroelectric properties with high piezoelectric charge coefficient (d_{33}) of 25 pm V^{-1}.[19a] The $FAPbBr_3$-PDMS composite film was grown onto an ITO-coated PET substrate, and then an Al film was deposited as the top electrode on the $FAPbBr_3$-PDMS layer to prepare the flexible piezoelectric generator (**Figure 6**a). The piezoelectric effect generates a positive voltage signal from the nanogenerator under a vertical compression, and the accumulated charges transport back in a reverse direction when the vertical compression is released, as shown in Figure 6b. The flexible device exhibits high performance with a piezoelectric output voltage of 8.5 V and current density of 3.8 μA cm^{-2} under periodically vertical compression and release operations (Figure 6c).[19a] Furthermore, a ferroelectric $FAPbBr_3$ perovskite-based nanogenerator was optimized by using piezoelectric polymer of poly vinylidene fluoride (PVDF), and the nanogenerator with PET/Cr/Au/$FAPbBr_3$ + PVDF/Au/Cr/PET configuration showed the current density of 6.2 μA cm^{-2} and output voltage of 30 V (Figure 6d).[65] In another report, Zhang et al. applied $FAPbBr_3$ nanocrystals (NCs) into perovskite LEDs and piezoelectric nanogenerators. They found that the power produced by these nanogenerators can be collected in capacitors and then drive LEDs.[66]

According to the calculations, $CsPbBr_3$ can be transformed to a ferroelectric phase with tetragonal P4*mm* symmetry and a P_s of 23 μC cm^{-2} under a pressure of 15 GPa and $CsPbF_3$ may be ferroelectric with rhombohedral *R3c* symmetry (Table 1).[67] Recently, Kim and Stroppa et al. predicted in theory that $FASnI_3$ is also ferroelectric phase with an orthorhombic A*mm2* structure. Furthermore, in principle the reversal of the polar axis with an external electric field can switch spin texture in tetragonal $MAPbI_3$, $MASnI_3$, orthorhombic $MASbBr_3$, and $FASnI_3$ ferroelectrics through the existence of a strong spin-orbit coupling effect.[53,68] These predictions are very relevant to further study of the functionality of ferroelectric large polaron

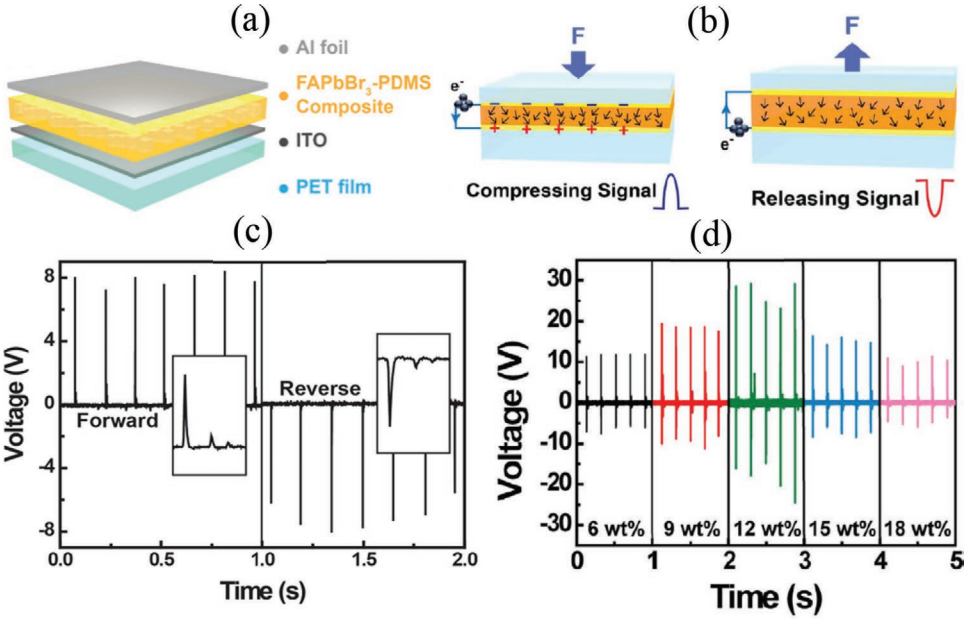

Figure 6. a) Structure sketch of PET/ITO/$FAPbBr_3$-PDMS/Al flexible piezoelectric nanogenerator, and b) schematic diagram of piezoelectric potential and electrons flow when the compressive force is applied or released from piezoelectric nanogenerator. c) Output voltage of the PET/ITO/$FAPbBr_3$-PDMS/Al nanogenerator. Reproduced with permission.[19a] Copyright 2016, WILEY-VCH Verlag GmbH & Co. KGaA, Weinheim. d) Output voltage of the PET/Cr/Au/$FAPbBr_{3-x}$ wt% PVDF/Au/Cr/PET nanogenerator. Reproduced with permission.[65] Copyright 2017, Elsevier Ltd.

on $CsPbBr_3$ and $FASnI_3$ semiconductors, which show excellent semiconducting properties and PCE as high as 8.9% and 7.78%, respectively.

4. Halide Perovskite Insulators with Strong Ferroelectricity

4.1. Ferroelectricity of MD–NH_4I_3 Crystal

As summarized in Table 1, several halide perovskite ferroelectrics have emerged with strong ferroelectric characteristics but poor semiconductor properties (e.g., low carrier mobility and short diffusion length). Halide perovskite materials that possess robust ferroelectric and piezoelectric properties have lots of potential for flexible and wearable electronic applications. In fact, the order-disorder transitions of cations in these halide perovskites around the BX_6 octahedra are responsible for symmetry breaking and ferroelectricity of these materials. The possibility of ferroelectric–paraelectric phase transition can be recognized by at least a twofold increase in dielectric constant with increasing the temperature. Moreover, the compound can be considered as either piezoelectric or pyroelectric if no dielectric anomaly is observed.[69] Ye et al. prepared *N*-methyl-*N*′-diazabicyclo[2.2.2]octonium–NH_4I_3 (i.e., MD–NH_4I_3) crystal with a relatively simple 3D structure (**Figure 7**a).[26] The crystal has rhombohedral R3 structure with crystal parameters of $a = b = c = 7.259$ Å and $\alpha = \beta = \gamma = 84.767°$ at room temperature. MD is positioned at the center in the unit cell, NH_4^+ groups stand at vertexes and I^- ions are at the centers of the edges. The high-level ferroelectric performance of (111) MD–NH_4I_3 crystal renders a P_s of 22 µC cm^{-2} at 448 K according to the *P*–*E* loops shown in Figure 7b and a piezoelectric d_{33} of ≈14 pC N^{-1} at room temperature. Such P_s value is comparable to barium titanate and much higher than PVDF.[11] Furthermore, both P_s and the effective second-order nonlinear optic susceptibility $\chi^{(2)}$ show the same trend with increasing temperature (Figure 7c), which is in accordance with the Landau relationship $\chi^{(2)} = 6\varepsilon_0\beta P_s$ where, β denotes an almost temperature independent coefficient.[70] There is an abrupt change in both P_s and $\chi^{(2)}$ near T_c due to the ferroelectric–paraelectric phase transition. MD–NH_4I_3 crystals have potential to be applied in biomedical devices, soft robotics, energy transduction, and other fields in the future.[71]

4.2. Ferroelectricity and Piezoelectricity of TC–$MnCl_3$ Crystal

Halide perovskite ferroelectric materials possess the advantages of flexible design, light weight, easy processing, and being environmentally friendly. Ferroelectrics are naturally piezoelectrics, because of lacking inversion center in their structures. However, the weak piezoelectric effect of these molecular ferroelectrics has remained a shortcoming for a long time. You et al. prepared trimethylchloromethyl ammonium (TC) trichloromanganese (II) (TC-$MnCl_3$) in aqueous solution at room temperature.[27] It has a centrosymmetric structure above T_c, that is, ≈405 K due to the orientational disorder of the organic cation. The crystal loses its centrosymmetry below T_c as a result of the "freezing" of cations, which induces the appearance of a spontaneous polarization in the monoclinic *Cc* phase (**Figure 8**a). The P_s is of 4.0 µC cm^{-2} according to their *P*–*E* loops in Figure 8b, in which the corresponding current density-bias voltage curves are illustrated as well. Polarization of TC-$MnCl_3$ only decreases less than 10% after 10^7 cycles of polarization switching. Besides, TC-$MnCl_3$ also presents a piezoelectric d_{33}

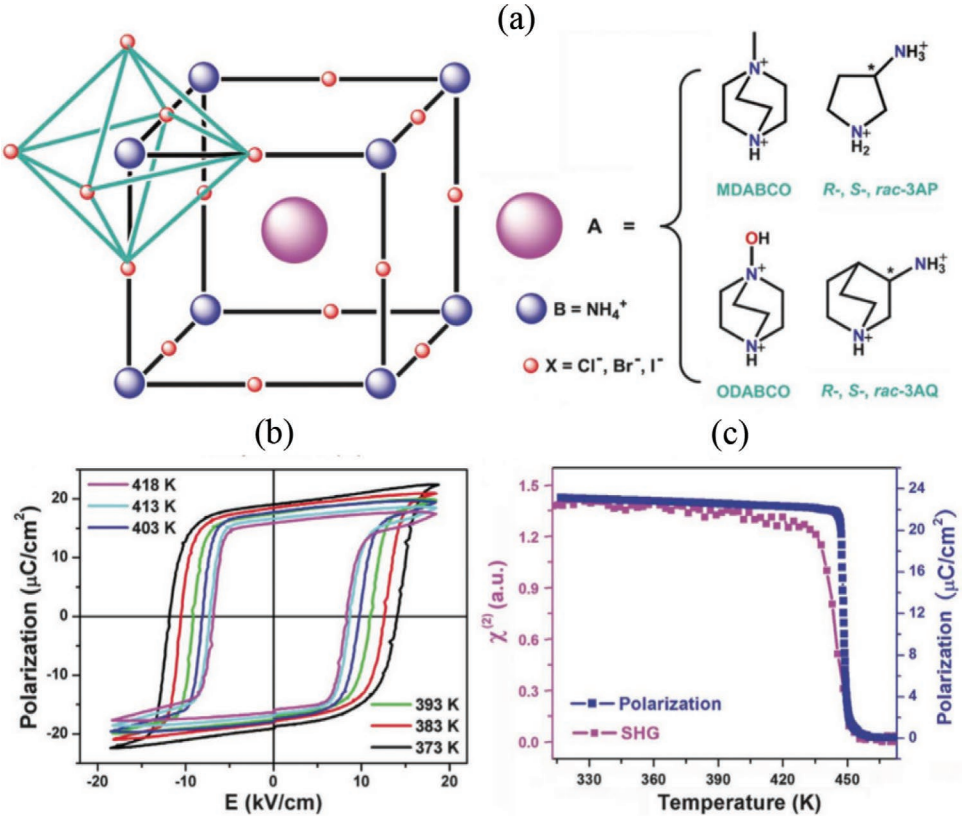

Figure 7. a) Structural and chemical structure of $A(NH_4)X_3$-type metal-free perovskite ferroelectric materials. b) *P–E* hysteresis loops of MD–NH_4I_3 at different temperatures. c) The relationship between second-order nonlinear optical coefficient $\chi^{(2)}$ and spontaneous polarization P_s versus temperature. Reproduced with permission.[26] Copyright 2018, American Association for the Advancement of Science (AAAS).

value of 185 pC N^{-1} along the proximity of the [102] direction of the crystal (Figure 8c), which is superior to most of the weak piezoelectric coefficients measured in organic materials.[72] The inset shows the d_{33} with fluctuation as little as <10 pC N^{-1} when the frequency of driving force ranges from 30 to 300 Hz. These high performances pave the path for the application of TC-$MnCl_3$ in micromechanical and biomechanical industries such as flexible devices and nanogenerators.

4.3. Ferroelectricity and Piezoelectricity of $(TF)_x(TC)_{1-x}CdCl_3$ Crystal

Based on the organic TC group, Liao et al. synthesized the molecular perovskite $(TF)_x(TC)_{1-x}CdCl_3$ (TF, trimethylfluoromethyl ammonium; $0 \le x \le 1$).[15] As shown in **Figure 9**a, with increasing of TF content (x) from 0.25 to 0.3, $(TF)_x(TC)_{1-x}CdCl_3$ stays in MPB region where the ferroelectric monoclinic phase (point group m, $0 \le x < 0.25$) and the ferroelectric hexagonal phase (point group 6*mm*, $0.3 < x \le 0.5$) coexists. The hexagonal phase (point group 6/m) lies in the region of $0.55 \le x \le 1$ at room temperature.[15] The MPB of monoclinic and hexagonal phases optimized their piezoelectric property. Piezoelectric coefficient d_{33} was obtained by PFM and the abrupt change at $x = 0.26$ verified the piezoelectricity near the MPB (Figure 9b). Besides, the Berlincourt method further confirmed the giant d_{33} of ≈1540 pC N^{-1} in $(TF)_{0.26}(TC)_{0.74}CdCl_3$ solid solution, which is as high as PZT piezoelectric ceramics. This makes it potentially useful for flexible piezoelectric applications. The maximum dielectric constant (ε') of $(TF)_{0.26}(TC)_{0.74}CdCl_3$ value is of ≈1500 at $T_c \approx 370$ K (Figure 9c). Moreover, $(TF)_x(TC)_{1-x}CdCl_3$ demonstrates well-saturated *P–E* hysteresis loops at $x \le 0.4$. Both P_s and remnant polarization (P_r) present the same tendency to increase slightly as x increases, showing the maximum values at $x = 0.26$ in the MPB region and then decreasing monotonously with x (Figure 9d).[15]

4.4. Ferroelectricity of 2D Lead Halide Perovskites

Some 2D multilayered lead halide perovskite ferroelectrics not only show strong ferroelectricity but also have a narrow band gap. In a multilayered lead halide perovskite $(A2)_2(A1)_{n-1}Pb_nX_{3n+1}$, A1 cation is the "perovskitizer" that occupies the central cavity of corner sharing PbX_6 octahedra and A2 cation is the "spacer" that is confined in the interlayer space of the inorganic sheets. In a representative work, Yang, et al. prepared 2D lead iodide perovskite ferroelectrics [*R*-1-(4-chlorophenyl) ethylammonium]$_2PbI_4$ (i.e., R_2PbI_4), [*S*-1-(4-chlorophenyl)ethylammonium]$_2PbI_4$ (i.e., S_2PbI_4), and (4,4-difl uorocyclohexylammonium)$_2PbI_4$ (i.e., D_2PbI_4).[28] The enantiomorphic structure of R_2PbI_4 is shown in **Figure 10**a. Similar to the structure of typical 2D perovskites such as $(C_4H_9NH_3)_2PbI_4$ and $(C_6H_5C_2H_4NH_3)_2PbI_4$,[73] corner-sharing PbI_6 octahedron

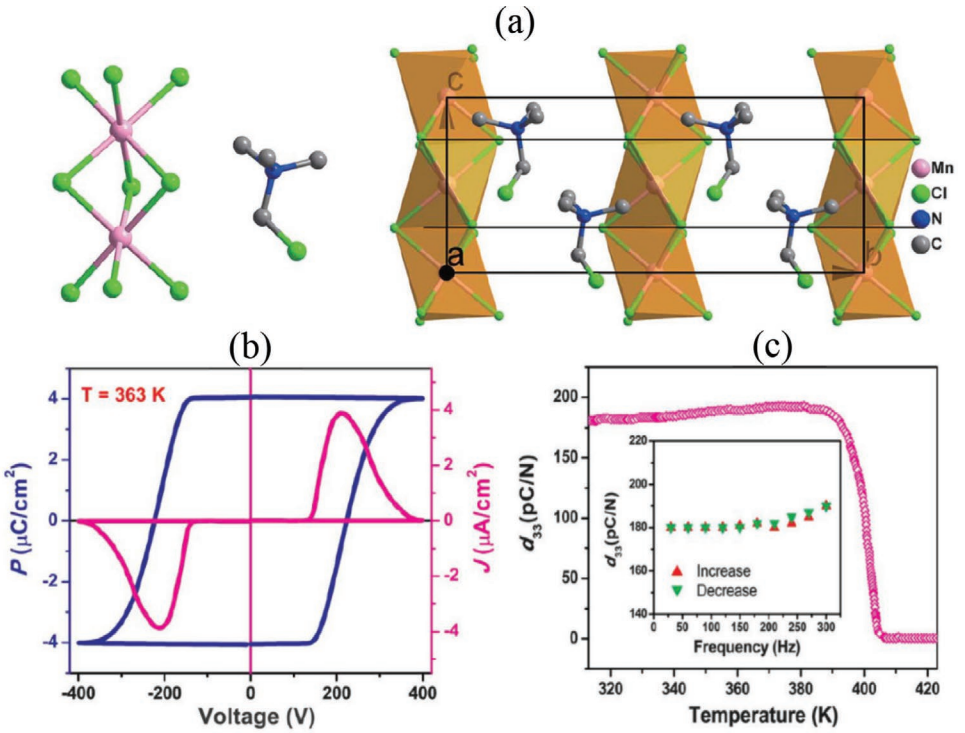

Figure 8. a) Schematic of ferroelectric TC-$MnCl_3$ structure, where the $MnCl_6$ octahedron coordination geometry and cationic structure are illustrated. The *c* axis vertical pseudo-mirror planes are outlined by the dark lines. b) Polarization versus bias voltage hysteresis loop and the corresponding current density-bias voltage curves. c) TC-$MnCl_3$ piezoelectric coefficient (d_{33}) versus temperature and frequency. Reproduced with permission.[27] Copyright 2017, AAAS.

layers are separated by 1-(4-chlorophenyl)ethylammonium cationic bilayers. Besides, these 2D perovskites possess semiconductor characteristics with a direct bandgap of 2.34 eV. The ferroelectric phases of S_2PbI_4 and R_2PbI_4 appear below 483 and 473.2 K, respectively. Figure 10b presents the PFM phase image of R_2PbI_4 film, indicating that the herringbone-shaped ferroelectric domains are formed by four kinds of domains that have different polarization directions, revealing its multiaxial ferroelectric nature.[27] Besides, there is an 180° change of phase angle in the bias dependence data. In fact, such switchable polarization is a compelling evidence of ferroelectricity (Figure 10c). Most importantly, R_2PbI_4 possesses a direct bandgap of 2.38 eV.[28] Furthermore, the ferroelectric polarization switching can change the direction of photovoltaic current. Owing to their unique properties, 2D lead iodide perovskite ferroelectrics are expected to be utilized in high-performance applications in future.[74]

4.5. Other Halide Perovskite Ferroelectrics

Recently, it was reported that hexagonal stacking perovskite-type complex (3-pyrrolinium)($CdCl_3$) shows P_s = 5.1 μC cm^{-2} below its T_c of 316 K.[75] The 1 mm-thick bulky crystal shows a V_{OC} as high as 32 V. Besides, (Pyrrolidinium)$MnBr_3$ and (3-ammoniopyrrolidinium)$RbBr_3$ are molecular pyrrolinium-based materials exhibiting attractive ferroelectric properties.[76] (Pyrrolidinium)$MnBr_3$ belongs to the 2-H stacking perovskite structure which is tunable through tailoring some templating cations or bridging atoms. It possesses intense red luminescence under UV excitation and 640 nm photoluminescence emission with a quantum efficiency around 28.5%. Moreover, (3-ammoniopyrrolidinium)$RbBr_3$ is a thermally stable ferroelectric candidate with a T_c as high as 440 K. More importantly, the compound has multiple polar axes, resulting in a large macroscopic polarization in the polycrystalline sample. As another attractive feature, the fast polarization reversal of >20 kHz is favorable for high-speed devices.[77]

Besides 3D and 2D halide perovskites, 1D halide perovskites, consisting of chains of metal halide octahedra surrounded by insulating organic cations, have presented remarkable properties due to site isolation and quantum confinement effects. Some 0D perovskites with the chemical formula of A_4BX_6 (A = monovalent organic cations, BX_6 = metal halide octahedra) have also shown ferroelectric properties due to the rotation of organic cations, making them suitable for electronic applications such as switchable memory devices.[78] However, the issue of low conductivity as a result of the existence of insulating organic cations between separated metal-halide octahedra have to be addressed in order to improve the utilization of low-dimensional halide perovskites.[79] Seo et al. reported that $(C_4H_9NH_3)(MA)_{n-1}Pb_nI_{3n+1}$ exhibited resistive switching behavior,[80] and they claimed that there was a decrease in device performance with increasing the dimension of the structures due to the change of bandgap. Clearly, in order to further advance this field, potential design rules should be developed to engineer the molecular structure, particularly the organic cations since they are strongly correlated to the ferroelectric

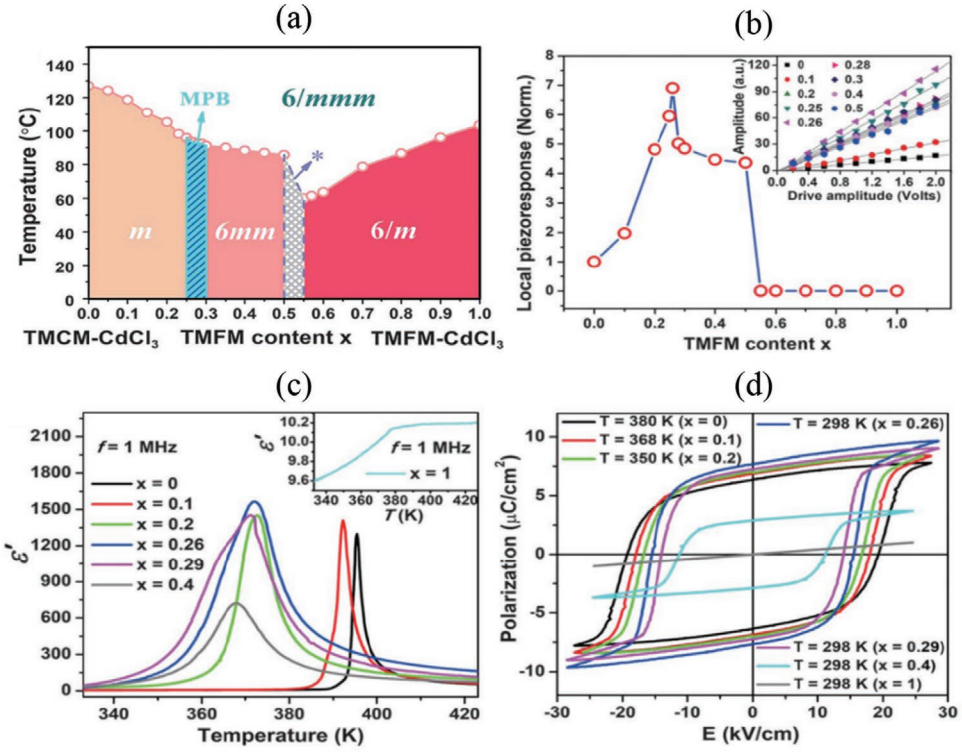

Figure 9. a) Phase diagram and point groups of different x ($0 \le x \le 1$) in $(TF)_x(TC)_{1-x}CdCl_3$, where the MPB region exists at $0.2 < x < 0.3$. b) Local piezoresponses as a function of composition. The inset demonstrates the dependence of piezoresponse amplitude on driving voltage at $x = 0$–0.5. c) Temperature dependence of ε' at 1 MHz for different x values. d) P–E hysteresis loops of several compositions. Reproduced with permission.[15] Copyright 2019, AAAS.

dipoles. The dynamic domain nucleation and polarization switch should also be investigated, as reported on some organic and oxide ferroelectrics.[81]

There have been few studies on the ferroelectric properties of halide perovskites when the materials are fabricated down to nanoscale. There is a possibility of disappearing of ferroelectricity in small scales as a result of decreasing long-range ordering of dipoles.[82] In fact, the existence of vortex domains followed by a toroidal ordering of dipoles may lead to zero net polarization in small ferroelectric nanoparticles.[83] Moreover, ferroelectricity can be limited by other parameters such as mechanical and electrical boundary conditions or the quality of nanomaterials.[84] On the other hand, DFT calculations have indicated that some absorbates such as carboxylates and OH can stabilize ferroelectricity in nanowires by screening polarization charges on the surfaces and therefore reducing the depolarization field.[85] Generally, it is important to obtain a complete understanding of the molecular structure design and ferroelectric behavior of these novel materials in order to promote halide perovskites in future electronic and electromechanical applications.

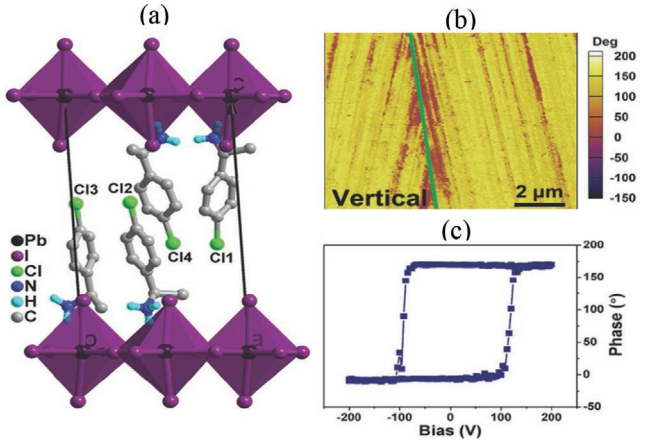

Figure 10. a) Crystal structures of a 2D lead iodide perovskite ferroelectric, that is, R_2PbI_4. b) Vertical PFM phase image. c) Room temperature vertical PFM phase signal versus the tip voltage bias at a selected point. Reproduced with permission.[28] Copyright 2019, WILEY-VCH Verlag GmbH & Co. KGaA, Weinheim.

5. Conclusions and Future Perspectives

In summary, two types of halide perovskite ferroelectrics have been reviewed, that is, perovskite semiconductors with weak ferroelectricity and insulating ferroelectrics with strong piezoelectricity. For the first type of halide perovskites prepared in aqueous solution near room temperature, the ferroelectric large polaron model is employed to explain how carriers are protected from scattering by charged defects. $MAPbI_3$, Fe- or Br-doped $MAPbI_3$, and $FAPbBr_3$ are the most representatives of halide perovskite ferroelectrics. As ferroelectricity is difficult to be recognized by macroscopic methods in these

typical semiconductors, most of researches characterized ferroelectric properties of these perovskites using microscopic methods such as PFM.[9,12,15] The second type of ferroelectric halide perovskites also have great potential for applications and are fundamentally interesting. MD–NH_4I_3, TC-$MnCl_3$ and $(TF)_x(TC)_{1-x}CdCl_3$ show large ferroelectric polarization and high piezoelectric d_{33} coefficient according to recent reports.[15,26,27] Especially, the $(TF)_{0.26}(TC)_{0.74}CdCl_3$ solid solution has MPB of monoclinic and hexagonal phases, which contributes to a giant d_{33} value of ≈1540 pC N^{-1}, being as high as that of PZT piezoelectric ceramics. Furthermore, there are ferroelectrics which belong to the family of multilayered halide perovskites with formula of $(A2)_2(A1)_{n-1}Pb_nX_{3n+1}$, such as R_2PbI_4, S_2PbI_4, D_2PbI_4, $EA_4Pb_3Br_{10}$, and $(EA)_2(MA)_2Pb_3Br_{10}$.[25,28] Some of them have a relatively narrow bandgap and the photovoltaic current can be reversed by switching their ferroelectric polarization. Their unusual ferroelectricity and piezoelectric properties can be exploited in optical, mechanical, and energy transduction applications. As a great advantage, halide perovskite ferroelectrics provides plenty of room for exploration and engineering in terms of material design.

Although extensively studied, the development of halide perovskite ferroelectrics is still at its infancy stage compared to their inorganic perovskite counterparts. In future, researchers should pay more attentions to at least five directions of advancing halide perovskite ferroelectrics regarding theoretical mechanisms, material properties, chemical and electrical stability, environmental friendliness, and new high value-added applications. 1) The mechanisms of these halide perovskite ferroelectrics still need to be elucidated. It is still not very clear how carriers are protected from scattering in halide perovskite semiconductors, which have much higher density of charged defects than those of conventional semiconductors such as high-purity Si and GaAs. Design rules are also needed to engineer the molecular structure, particularly the organic cations, to enhance ferroelectric dipoles and stability for practical applications. Insights on the mechanisms will facilitate the design of halide perovskites with high carrier mobility, wide band gap, and large polarization coexisting simultaneously. 2) It is necessary to design and prepare more halide perovskite materials with excellent semiconductor and ferroelectric properties. More systems of these materials should be explored with a focus on trying different organic groups with rationally selected metal ions and halogens to obtain a better device performance. 3) Most of the halide perovskites can be prepared in aqueous solution near room temperature. Some of them are not stable and even decompose in humid environment, high-temperature ambience, and/or under high light illumination. It is very important to further improve the chemical and electrical stability of halide perovskite ferroelectrics in order to use these materials widely in industries. 4) Pb element is not environmentally friendly and Pb-acid cells are pollutant sources. To substantially decrease or completely avoid the use of Pb element should be the precondition for new solar cells to be commercially viable, thus it would be desirable to develop high-performance solar cells on the base of Pb-free halide perovskite materials. 5) In addition to solar cells, LED, optical detectors, piezoelectric sensors, some high-value and high-quality cost-effective devices such as ferroelectric transistors, ferroelectric tunnel junctions, and multiferroic devices should be developed as urgent tasks.[86] As the range of applications expands, halide perovskites can find some niche areas with the possibility of substantial cost reduction and product recycling. Furthermore, these halide perovskite ferroelectrics are soft and flexible enough to be applied in wearable sensors and photoacoustic devices.[87] By leveraging on the rapid achievements recently achieved, researchers will be able to improve the mechanical and electrical properties of halide ferroelectric perovskites to further advancing their applications.

Acknowledgements

S.S. and W.G. contributed equally to this work. The works of G.L.Y. and J.M.L. were supported by the National Natural Science Foundation of China (51790492, 51721001 and 61874055) and the National Key Research Program of China (2016YFA0300101). This work was also supported by the Australian Research Council (DP190103316 and DP170103514).

Conflict of Interest

The authors declare no conflict of interest.

Keywords

ferroelectrics, ferroelectric semiconductors, halide perovskites, perovskite solar cells, piezoelectrics

Received: February 27, 2020
Revised: March 29, 2020
Published online:

[1] H. J. L. Megaw, *Ferroelectricity in Crystals*, Methuen, London, UK **1957**.
[2] a) W. Gao, L. You, Y. Wang, G. Yuan, Y.-H. Chu, Z. Liu, J.-M. Liu, *Adv. Electron. Mater.* **2017**, *3*, 1600542; b) Z. Zhang, P.-F. Li, Y.-Y. Tang, A. J. Wilson, K. Willets, M. Wuttig, R.-G. Xiong, S. Ren, *Sci. Adv.* **2017**, *3*, e1701008.
[3] T. M. Brenner, D. A. Egger, L. Kronik, G. Hodes, D. J. N. R. M. Cahen, *Nat. Rev. Mater.* **2016**, *1*, 15007.
[4] M. Déri, *Ferroelectric Ceramics*, Akadémiai Kiadó, Budapest **1966**.
[5] a) G. R. Love, *J. Am. Ceram. Soc.* **1990**, *73*, 323; b) V. S. Puli, D. K. Pradhan, D. B. Chrisey, M. Tomozawa, G. L. Sharma, J. F. Scott, R. S. Katiyar, *J. Mater. Sci.* **2013**, *48*, 2151; c) Q. Yuan, F. Yao, Y. Wang, R. Ma, H. Wang, *J. Mater. Chem. C* **2017**, *5*, 9552.
[6] a) Y. Lee, J. Park, S. Cho, Y.-E. Shin, H. Lee, J. Kim, J. Myoung, S. Cho, S. Kang, C. Baig, H. Ko, *ACS Nano* **2018**, *12*, 4045; b) V. V. Kochervinskii, *Russ. Chem. Rev.* **1999**, *68*, 821.
[7] Z. Zhang, R. Sakidja, F. Hu, B. Xu, S. Ren, *J. Phys. Chem. Lett.* **2019**, *10*, 206.
[8] C. A. P. de Araujo, L. D. McMillan, B. M. Melnick, J. D. Cuchiaro, J. F. Scott, *Ferroelectrics* **1990**, *104*, 241.
[9] W. Gao, L. Chang, H. Ma, L. You, J. Yin, J. Liu, Z. Liu, J. Wang, G. Yuan, *NPG Asia Mater.* **2015**, *7*, e189.
[10] Y. Zhao, A. M. Nardes, K. Zhu, *Faraday Discuss.* **2014**, *176*, 301.
[11] S. Horiuchi, Y. Tokura, *Nat. Mater.* **2008**, *7*, 357.
[12] Y. Rakita, O. Bar-Elli, E. Meirzadeh, H. Kaslasi, Y. Peleg, G. Hodes, I. Lubomirsky, D. Oron, D. Ehre, D. Cahen, *Proc. Natl. Acad. Sci. USA* **2017**, *114*, E5504.

[13] M. N. F. Hoque, M. Yang, Z. Li, N. Islam, X. Pan, K. Zhu, Z. Fan, *ACS Energy Lett.* **2016**, *1*, 142.
[14] a) V. G. Koukhar, N. A. Pertsev, R. Waser, *Phys. Rev. B* **2001**, *64*, 214103; b) A. Pecchia, D. Gentilini, D. Rossi, M. A. der Maur, A. di Carlo, *Nano Lett.* **2016**, *16*, 988.
[15] W.-Q. Liao, D. Zhao, Y.-Y. Tang, Y. Zhang, P.-F. Li, P.-P. Shi, X.-G. Chen, Y.-M. You, R.-G. Xiong, *Science* **2019**, *363*, 1206.
[16] J. Xiao, J. Chang, B. Li, F. H. Isikgor, D. Wang, Z. Fan, Z. Lin, J. Ouyang, K. Zeng, J. Chen, *J. Mater. Chem. A* **2018**, *6*, 9665.
[17] a) Q. Chen, H. Zhou, Y. Fang, A. Z. Stieg, T. B. Song, H. H. Wang, X. Xu, Y. Liu, S. Lu, J. You, P. Sun, J. McKay, M. S. Goorsky, Y. Yang, *Nat. Commun.* **2015**, *6*, 7269; b) S. Lai, Z. Yang, J. Li, B. Shao, J. Yang, Y. Wang, J. Qiu, Z. Song, *J. Mater. Chem. C* **2015**, *3*, 7699.
[18] S. Ippili, V. Jella, J. Kim, S. Hong, S.-G. Yoon, *Nano Energy* **2018**, *49*, 247.
[19] a) R. Ding, H. Liu, X. Zhang, J. Xiao, R. Kishor, H. Sun, B. Zhu, G. Chen, F. Gao, X. Feng, J. Chen, X. Chen, X. Sun, Y. Zheng, *Adv. Funct. Mater.* **2016**, *26*, 7708; b) A. A. Zhumekenov, M. I. Saidaminov, M. A. Haque, E. Alarousu, S. P. Sarmah, B. Murali, I. Dursun, X.-H. Miao, A. L. Abdelhady, T. Wu, O. F. Mohammed, O. M. Bakr, *ACS Energy Lett.* **2016**, *1*, 32.
[20] X. Meng, J. Lin, X. Liu, X. He, Y. Wang, T. Noda, T. Wu, X. Yang, L. Han, *Adv. Mater.* **2019**, *31*, 1903721.
[21] W. Chen, J. Zhang, G. Xu, R. Xue, Y. Li, Y. Zhou, J. Hou, Y. Li, *Adv. Mater.* **2018**, *30*, 1800855.
[22] E. H. Smith, N. A. Benedek, C. J. Fennie, *Inorg. Chem.* **2015**, *54*, 8536.
[23] X. Zhang, M. Zhang, G. Lu, *J. Phys. Chem. C* **2016**, *120*, 23969.
[24] S. Wang, X. Liu, L. Li, C. Ji, Z. Sun, Z. Wu, M. Hong, J. Luo, *J. Am. Chem. Soc.* **2019**, *141*, 7693.
[25] X. Liu, S. Wang, P. Long, L. Li, Y. Peng, Z. Xu, S. Han, Z. Sun, M. Hong, J. Luo, *Angew. Chem., Int. Ed.* **2019**, *58*, 14504.
[26] H.-Y. Ye, Y.-Y. Tang, P.-F. Li, W.-Q. Liao, J.-X. Gao, X.-N. Hua, H. Cai, P.-P. Shi, Y.-M. You, R.-G. Xiong, *Science* **2018**, *361*, 151.
[27] Y.-M. You, W.-Q. Liao, D. Zhao, H.-Y. Ye, Y. Zhang, Q. Zhou, X. Niu, J. Wang, P.-F. Li, D.-W. Fu, Z. Wang, S. Gao, K. Yang, J.-M. Liu, J. Li, Y. Yan, R.-G. Xiong, *Science* **2017**, *357*, 306.
[28] C.-K. Yang, W.-N. Chen, Y.-T. Ding, J. Wang, Y. Rao, W.-Q. Liao, Y.-Y. Tang, P.-F. Li, Z.-X. Wang, R.-G. Xiong, *Adv. Mater.* **2019**, *31*, 1808088.
[29] T.-T. Sha, Y.-A. Xiong, Q. Pan, X.-G. Chen, X.-J. Song, J. Yao, S.-R. Miao, Z.-Y. Jing, Z.-J. Feng, Y.-M. You, R.-G. Xiong, *Adv. Mater.* **2019**, *31*, 1901843.
[30] B. Chen, Z. Zuo, Y. Liu, Q.-F. Zhan, Y. Xie, H. Yang, G. Dai, Z. Li, G. Xu, R.-W. Li, *Appl. Phys. Lett.* **2012**, *100*, 173903.
[31] A. Zenkevich, Y. Matveyev, K. Maksimova, R. Gaynutdinov, A. Tolstikhina, V. Fridkin, *Phys. Rev. B* **2014**, *90*, 161409.
[32] W. Ji, K. Yao, Y. C. Liang, *Adv. Mater.* **2010**, *22*, 1763.
[33] R. Nechache, C. Harnagea, S. Li, L. Cardenas, W. Huang, J. Chakrabartty, F. Rosei, *Nat. Photonics* **2015**, *9*, 61.
[34] a) W. Gao, R. Brennan, Y. Hu, M. Wuttig, G. Yuan, E. Quandt, S. Ren, *Mater. Today* **2018**, *21*, 771; b) W. Gao, Z. Zhang, P.-F. Li, Y.-Y. Tang, R.-G. Xiong, G. Yuan, S. Ren, *ACS Nano* **2017**, *11*, 11739; c) W. Zhang, R.-G. Xiong, *Chem. Rev.* **2012**, *112*, 1163.
[35] a) G. Gautschi, in *Piezoelectric Sensorics*, Springer, New York **2002**, p. 73; b) M. A. Khan, M. A. Nadeem, H. Idriss, *Surf. Sci. Rep.* **2016**, *71*, 1.
[36] R. B. Meyer, L. Liebert, L. Strzelecki, P. Keller, *J. Phys., Lett.* **1975**, *36*, 69.
[37] E. Soergel, *Appl. Phys. B* **2005**, *81*, 729.
[38] B. Huang, G. Kong, E. N. Esfahani, S. Chen, Q. Li, J. Yu, N. Xu, Y. Zhang, S. Xie, H. Wen, P. Gao, J. Zhao, J. Li, *npj Quantum Mater.* **2018**, *3*, 30.
[39] a) C. Lu, M. Wu, L. Lin, J.-M. Liu, *Natl. Sci. Rev.* **2019**, *6*, 653; b) H. Pang, F. Zhang, M. Zeng, X. Gao, M. Qin, X. Lu, J. Gao, J. Dai, Q. Li, *npj Quantum Mater.* **2016**, *1*, 16015; c) Y. S. Tang, S. M. Wang, L. Lin, C. Li, S. H. Zheng, C. F. Li, J. H. Zhang, Z. B. Yan, X. P. Jiang, J. M. Liu, *Phys. Rev. B* **2019**, *100*, 134112.
[40] H. T. Yi, X. Wu, X. Zhu, V. Podzorov, *Adv. Mater.* **2016**, *28*, 6509.
[41] a) M. M. Lee, J. Teuscher, T. Miyasaka, T. N. Murakami, H. J. Snaith, *Science* **2012**, *338*, 643; b) K. Miyata, D. Meggiolaro, M. T. Trinh, P. P. Joshi, E. Mosconi, S. C. Jones, F. de Angelis, X. Y. Zhu, *Sci. Adv.* **2017**, *3*, e1701217; c) K. Miyata, X. Y. Zhu, *Nat. Mater.* **2018**, *17*, 379; d) S. D. Stranks, G. E. Eperon, G. Grancini, C. Menelaou, M. J. P. Alcocer, T. Leijtens, L. M. Herz, A. Petrozza, H. J. Snaith, *Science* **2013**, *342*, 341.
[42] Q. Dong, Y. Fang, Y. Shao, P. Mulligan, J. Qiu, L. Cao, J. Huang, *Science* **2015**, *347*, 967.
[43] H. Zhu, M. T. Trinh, J. Wang, Y. Fu, P. P. Joshi, K. Miyata, S. Jin, X. Y. Zhu, *Adv. Mater.* **2017**, *29*, 1603072.
[44] A. K. Jena, A. Kulkarni, T. Miyasaka, *Chem. Rev.* **2019**, *119*, 3036.
[45] Z. Zhang, Z. Li, S. Chang, W. Gao, G. Yuan, R.-G. Xiong, S. Ren, *Mater. Today* **2019**, https://doi.org/10.1016/j.mattod.2019.09.004.
[46] L. Li, P. A. Salvador, G. S. Rohrer, *Nanoscale* **2014**, *6*, 24.
[47] S. Singh, A. L. Sangle, T. Wu, N. Khare, J. L. MacManus-Driscoll, *ACS Appl. Mater. Interfaces* **2019**, *11*, 45683.
[48] S. Wang, L. Li, W. Weng, C. Ji, X. Liu, Z. Sun, W. Lin, M. Hong, J. Luo, *J. Am. Chem. Soc.* **2020**, *142*, 55.
[49] L. Wang, H. Ma, L. Chang, C. Ma, G. Yuan, J. Wang, T. Wu, *Small* **2017**, *13*, 1602355.
[50] I. Anusca, S. Balciunas, P. Gemeiner, S. Svirskas, M. Sanlialp, G. Lackner, C. Fettkenhauer, J. Belovickis, V. Samulionis, M. Ivanov, B. Dkhil, J. Banys, V. V. Shvartsman, D. C. Lupascu, *Adv. Energy Mater.* **2017**, *7*, 1700600.
[51] A. M. A. Leguy, J. M. Frost, A. P. McMahon, V. G. Sakai, W. Kockelmann, C. Law, X. Li, F. Foglia, A. Walsh, B. C. O'Regan, J. Nelson, J. T. Cabral, P. R. F. Barnes, *Nat. Commun.* **2015**, *6*, 7124.
[52] E. J. Juarez-Perez, R. S. Sanchez, L. Badia, G. Garcia-Belmonte, Y. S. Kang, I. Mora-Sero, J. Bisquert, *J. Phys. Chem. Lett.* **2014**, *5*, 2390.
[53] A. Stroppa, D. di Sante, P. Barone, M. Bokdam, G. Kresse, C. Franchini, M.-H. Whangbo, S. J. N. c. Picozzi, *Nat. Commun.* **2014**, *5*, 5900.
[54] Y. Zhang, W. Jie, P. Chen, W. Liu, J. Hao, *Adv. Mater.* **2018**, *30*, 1707007.
[55] H. Röhm, T. Leonhard, M. J. Hoffmann, A. Colsmann, *Energy Environ. Sci.* **2017**, *10*, 950.
[56] R. López-Juárez, O. Novelo-Peralta, F. González-García, F. Rubio-Marcos, M.-E. Villafuerte-Castrejón, *J. Eur. Ceram. Soc.* **2011**, *31*, 1861.
[57] S. Liu, F. Zheng, N. Z. Koocher, H. Takenaka, F. Wang, A. M. Rappe, *J. Phys. Chem. Lett.* **2015**, *6*, 693.
[58] F. Z. Bi, S. Markov, R. L. Wang, Y. H. Kwok, W. J. Zhou, L. M. Liu, X. Zheng, G. H. Chen, C. Y. Yam, *J. Phys. Chem. C* **2017**, *121*, 11151.
[59] J. M. Frost, K. T. Butler, F. Brivio, C. H. Hendon, M. van Schilfgaarde, A. Walsh, *Nano Lett.* **2014**, *14*, 2584.
[60] C.-C. Zhang, Z.-K. Wang, S. Yuan, R. Wang, M. Li, M. F. Jimoh, L.-S. Liao, Y. Yang, *Adv. Mater.* **2019**, *31*, 1902222.
[61] A. Stroppa, C. Quarti, F. de Angelis, S. Picozzi, *J. Phys. Chem. Lett.* **2015**, *6*, 2223.
[62] E. Mosconi, A. Amat, M. K. Nazeeruddin, M. Grätzel, F. de Angelis, *J. Phys. Chem. C* **2013**, *117*, 13902.
[63] J. H. Noh, S. H. Im, J. H. Heo, T. N. Mandal, S. I. Seok, *Nano Lett.* **2013**, *13*, 1764.
[64] a) B. Chen, J. Shi, X. Zheng, Y. Zhou, K. Zhu, S. Priya, *J. Mater. Chem. A* **2015**, *3*, 7699; b) H. Ishihara, S. Sarang, Y.-C. Chen, O. Lin, P. Phummirat, L. Thung, J. Hernandez, S. Ghosh, V. Tung, *J. Mater. Chem. A* **2016**, *4*, 6989.
[65] R. Ding, X. Zhang, G. Chen, H. Wang, R. Kishor, J. Xiao, F. Gao, K. Zeng, X. Chen, X. W. Sun, Y. Zheng, *Nano Energy* **2017**, *37*, 126.

[66] X. Zhang, R. Ding, X. W. Sun, *SID Int. Symp. Dig. Tech. Pap.* **2019**, *50*, 1669.
[67] a) M. Rodová, J. Brožek, K. Knížek, K. Nitsch, *J. Therm. Anal. Calorim.* **2003**, *71*, 667; b) C. C. Stoumpos, C. D. Malliakas, J. A. Peters, Z. Liu, M. Sebastian, J. Im, T. C. Chasapis, A. C. Wibowo, D. Y. Chung, A. J. Freeman, B. W. Wessels, M. G. Kanatzidis, *Cryst. Growth Des.* **2013**, *13*, 2722.
[68] M. Kim, J. Im, A. J. Freeman, J. Ihm, H. Jin, *Proc. Natl. Acad. Sci. USA* **2014**, *111*, 6900.
[69] P.-P. Shi, Y.-Y. Tang, P.-F. Li, W.-Q. Liao, Z.-X. Wang, Q. Ye, R.-G. Xiong, *Chem. Soc. Rev.* **2016**, *45*, 3811.
[70] H. L. Cai, W. Zhang, J. Z. Ge, Y. Zhang, K. Awaga, T. Nakamura, R. G. Xiong, *Phys. Rev. Lett.* **2011**, *107*, 147601.
[71] a) Z. Zhang, H. Li, R. Miller, H. Malissa, S. Jamali, C. Boehme, J. C. Grossman, S. Ren, *Nano Lett.* **2018**, *18*, 4346; b) Z. Zhang, R. C. Remsing, H. Chakraborty, W. Gao, G. Yuan, M. L. Klein, S. Ren, *Proc. Natl. Acad. Sci. USA* **2018**, *115*, 3776.
[72] a) Z. Fan, K. Sun, J. Wang, *J. Mater. Chem. A* **2015**, *3*, 18809; b) W. Li, Z. Wang, F. Deschler, S. Gao, R. H. Friend, A. K. Cheetham, *Nat. Rev. Mater.* **2017**, *2*, 16099.
[73] J. Hu, L. Yan, W. You, *Adv. Mater.* **2018**, *30*, 1802041.
[74] Z. Zhang, Y. Yu, Y. Tang, Y.-s. Guan, Y. Hu, J. Yin, K. Willets, S. Ren, *Adv. Electron. Mater.* **2019**, *6*, 1900929.
[75] H.-Y. Ye, Y. Zhang, D.-W. Fu, R.-G. Xiong, *Angew. Chem., Int. Ed.* **2014**, *53*, 11242.
[76] Y. Zhang, W.-Q. Liao, D.-W. Fu, H.-Y. Ye, C.-M. Liu, Z.-N. Chen, R.-G. Xiong, *Adv. Mater.* **2015**, *27*, 3942.
[77] Q. Pan, Z.-B. Liu, Y.-Y. Tang, P.-F. Li, R.-W. Ma, R.-Y. Wei, Y. Zhang, Y.-M. You, H.-Y. Ye, R.-G. Xiong, *J. Am. Chem. Soc.* **2017**, *139*, 3954.
[78] H. Lin, C. Zhou, Y. Tian, T. Siegrist, B. Ma, *ACS Energy Lett.* **2018**, *3*, 54.
[79] J. Zhang, X. Yang, H. Deng, K. Qiao, U. Farooq, M. Ishaq, F. Yi, H. Liu, J. Tang, H. Song, *Nano-Micro Lett.* **2017**, *9*, 36.
[80] J.-Y. Seo, J. Choi, H.-S. Kim, J. Kim, J.-M. Yang, C. Cuhadar, J. S. Han, S.-J. Kim, D. Lee, H. W. Jang, N.-G. Park, *Nanoscale* **2017**, *9*, 15278.
[81] a) W. Hu, Z. Wang, Y. Du, X.-X. Zhang, T. Wu, *ACS Appl. Mater. Interfaces* **2014**, *6*, 19057; b) H. Ma, W. Gao, J. Wang, T. Wu, G. Yuan, J. Liu, Z. Liu, *Adv. Electron. Mater.* **2016**, *2*, 1600038; c) H. Ma, G. Yuan, T. Wu, Y. Wang, J.-M. Liu, *ACS Appl. Mater. Interfaces* **2018**, *10*, 40911; d) T. S. Yoo, S. A. Lee, C. Roh, S. Kang, D. Seol, X. Guan, J.-S. Bae, J. Kim, Y.-M. Kim, H. Y. Jeong, S. Jeong, A. Y. Mohamed, D.-Y. Cho, J. Y. Jo, S. Park, T. Wu, Y. Kim, J. Lee, W. S. Choi, *ACS Appl. Mater. Interfaces* **2018**, *10*, 41471.
[82] P. M. Rørvik, T. Grande, M.-A. Einarsrud, *Adv. Mater.* **2011**, *23*, 4007.
[83] I. Naumov, H. Fu, *Phys. Rev. Lett.* **2007**, *98*, 077603.
[84] C. Lichtensteiger, M. Dawber, J.-M. Triscone, in *Physics of Ferroelectrics: A Modern Perspective*, Topics in Applied Physics, vol. 105, Springer, Berlin **2007**.
[85] J. E. Spanier, A. M. Kolpak, J. J. Urban, I. Grinberg, L. Ouyang, W. S. Yun, A. M. Rappe, H. Park, *Nano Lett.* **2006**, *6*, 735.
[86] a) W. J. Hu, T. R. Paudel, S. Lopatin, Z. Wang, H. Ma, K. Wu, A. Bera, G. Yuan, A. Gruverman, E. Y. Tsymbal, T. Wu, *Adv. Funct. Mater.* **2018**, *28*, 1704337; b) W. Jin Hu, Z. Wang, W. Yu, T. Wu, *Nat. Commun.* **2016**, *7*, 10808; c) L. Liao, H. J. Fan, B. Yan, Z. Zhang, L. L. Chen, B. S. Li, G. Z. Xing, Z. X. Shen, T. Wu, X. W. Sun, J. Wang, T. Yu, *ACS Nano* **2009**, *3*, 700; d) L. Ren, M. Wang, X. Guan, S. Wang, H. Yan, Z. Zhang, G. Yuan, T. Wu, K. Jin, *Adv. Opt. Mater.* **2019**, *7*, 1901092; e) L. You, C. Lu, P. Yang, G. Han, T. Wu, U. Luders, W. Prellier, K. Yao, L. Chen, J. Wang, *Adv. Mater.* **2010**, *22*, 4964; f) M. A. Zurbuchen, T. Wu, S. Saha, J. Mitchell, S. K. Streiffer, *Appl. Phys. Lett.* **2005**, *87*, 232908.
[87] D. B. Velusamy, M. A. Haque, M. R. Parida, F. Zhang, T. Wu, O. F. Mohammed, H. N. Alshareef, *Adv. Funct. Mater.* **2017**, *27*, 1605554.